Journal of Membrane Science Letters 2 (2022) 100019

Contents lists available at ScienceDirect

Journal of Membrane Science Letters

journal homepage: www.elsevier.com/locate/memlet

Fouling-Resistant Membranes with Tunable Pore Size Fabricated Using Cross-Linkable Copolymers with High Zwitterion Content

Samuel J. Lounder, Patrick T. Wright, Luca Mazzaferro, Ayse Asatekin*

Department of Chemical and Biological Engineering, Tufts University, Medford, MA 02155, USA

ARTICLE INFO

KEYWORDS:
Membranes
fouling resistant
zwitterions
cross-linking
tunable

ABSTRACT

This work describes a new approach for synthesizing extremely fouling-resistant, zwitterionic membranes with controlled, tunable pore sizes that extend from ion separations (< 1 nm) to the ultrafiltration range (~2 nm). These membranes are manufactured by the UV treatment of high zwitterion content amphiphilic copolymers with cross-linkable functionality to stabilize the membrane selective layers, preventing excessive swelling and dissolution of copolymers containing as high as 80 wt% zwitterionic repeat units. Zwitterion weight fraction allows the tuning of membrane performance, with effective pore size and permeance both increasing with zwitterion content. The high zwitterion content membranes were remarkably fouling-resistant and demonstrated a salt-responsive behavior not previously observed with self-assembling zwitterionic copolymer membranes.

Membrane filtration is an efficient, scalable, and low-footprint separation technology. However, membrane fouling, defined as the unwanted accumulation feed components onto the membrane surface or into the membrane pores, presents a critical challenge that severely limits their use in many applications. (Bruggen and Vandecasteele, 2003, Epsztein et al., 2020, Greenlee et al., 2009, Mauter et al., 2018, Shannon et al., 2008, Sholl and Lively, 2016, Zhang et al., 2016) Fouling leads to severe reductions in water permeability, necessitating expensive cleaning cycles, significantly limiting membrane lifetime, and oftentimes dominating the economic and technical feasibility for membrane systems. (Hurwitz et al., 2018, Esfahani et al., 2019, Ward et al., 2021) Membrane surface functionalization with zwitterions (ZIs), defined as molecules containing an equal number of positive and negative charges, (Maan et al., 2020, Laschewsky, 2014) through grafting (Bhattacharya and Misra, 2004, Susanto and Ulbricht, 2007, Shahkaramipour et al., 2017, Yang et al., 2011, Weinman et al., 2018) or blending (Kaner et al., 2019, Kaner et al., 2017, Sun et al., 2006, Zhao et al., 2013) can increase surface hydrophilicity and thus fouling resistance. Nevertheless, state-of-the-art commercial membranes still lack the fouling resistance needed to treat especially fouling-prone feedstocks.

Another important challenge is controlling the selectivity and effective pore size of membranes. (Epsztein et al., 2020, Sadeghi et al., 2018, Zhang et al., 2018, Sujanani et al., 2020) Manufacturing processes for most commercial membranes (e.g. non-solvent induced phase inversion, interfacial polymerization) involve a complex array of competing mass transfer processes along with phase separation and/or chemical reactions. (Sadeghi et al., 2018, Zhang et al., 2018, Guillen et al., 2011, Dong et al., 2020) As a result, controlling selectivity remains a "black art", relying on careful and consistent tuning of many process criteria during the manufacturing process.

Self-assembly of polymeric materials is a promising tool for addressing both of these challenges. (Sadeghi et al., 2018, Zhang et al., 2018, Lang et al., 2021, Moon et al., 2020, Hoffman and Phillip, 2020, Zhang et al., 2017) Well-designed self-assembly processes can offer better control over both the surface chemistry and nano-scale pore structure. (Sadeghi et al., 2018, Sadeghi and Asatekin, 2019, Qu et al., 2015, Zhang et al., 2021, Zhang et al., 2020, Dugas et al., 2020) For example, exceptionally fouling-resistant thin film composite (TFC) membranes have been prepared using random zwitterionic amphiphilic copolymers (r-ZACs), defined as random copolymers of hydrophobic and zwitterionic repeat units (Fig. 1). (Bengani et al., 2015, Bengani-Lutz et al., 2017, Bengani-Lutz et al., 2017, Lounder and Asatekin, 2021, Bengani-Lutz et al., 2019) Due to strong ZI-ZI interactions, r-ZACs can self-assemble to form zwitterionic nanochannels surrounded by a hydrophobic nanodomain. The hydrated zwitterionic nanochannels are permeable to water and solutes less than ~1.5 nm in hydrated diameter, the membrane size cut-off. This size-based selectivity is nearly universal for all r-ZAC membranes and shows little variation with ZI chemistry, (Bengani-Lutz et al., 2017) hydrophobic monomer chemistry, (Bengani et al., 2015) and ZI content (~30-50 wt%, up to solubility limit). (Bengani et al., 2015) Therefore, while the scalability and exceptional fouling resistance of r-ZAC membranes makes them attractive for numerous industrial wastewater treatment applications,

* Corresponding Author.
E-mail address: ayse.asatekin@tufts.edu (A. Asatekin).

https://doi.org/10.1016/j.memlet.2022.100019
Received 17 December 2021; Received in revised form 10 February 2022; Accepted 19 February 2022

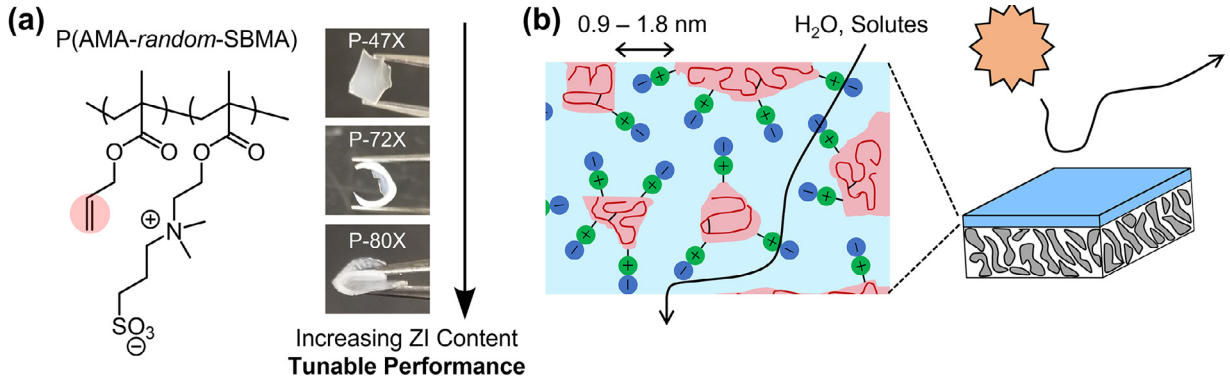

Fig. 1. (a) Chemical structure of the cross-linkable r-ZAC (x-ZAC) used in this work. The cross-linkable group is circled in pink. Photographs show x-ZAC films of varying composition swollen in water. Higher ZI content films were more flexible when swollen. (b) Schematic showing the fouling-resistant TFC membranes prepared using high ZI content x-ZACs. Copolymer cross-linking stabilized the x-ZAC selective layers in water. Increased permeance and effective pore size resulted from extensive water sorption that swelled the ZI domains.

novel approaches that tune membrane selectivity are required to access a broader range of separations.

Recently, we developed membranes with r-ZACs featuring cross-linkable functional groups (x-ZACs), and showed that cross-linking of the x-ZAC selective layer leads to controllable reductions in effective pore size. (Lounder and Asatekin, 2021, Lounder and Asatekin, 2021) The most highly cross-linked membranes had pore sizes as low as 0.9 nm, exhibiting exceptional interaction-based ion selectivity (Lounder and Asatekin, 2021) while maintaining excellent fouling resistance. (Lounder and Asatekin, 2021) However, the range of pore sizes accessible by this method was limited to the 0.9-1.4 nm range. The permeances of these membranes were also quite low, often below 1 L $m^{-2}hr^{-1}bar^{-1}$. There remains a need for broadening the separations accessible by x-ZAC membranes by increasing the upper-limit for effective pore size, and for improving the water permeance overall.

In this work, we address these two challenges through the cross-linking of x-ZACs containing as much as ~80 wt% ZI repeat units. While these high ZI content copolymers would normally be too hydrophilic to form water-stable TFC membranes, photo-cross-linking allowed the facile preparation of membranes with higher effective pore sizes, higher permeances, and further enhanced fouling resistance (Fig. 1). Furthermore, the high ZI content x-ZAC membranes exhibit ionic strength responsive behavior not previously observed with r-ZAC membranes of lower ZI fractions.

To synthesize the x-ZACs, we copolymerized allyl methacrylate (AMA) and sulfobetaine methacrylate (SBMA) via Activators ReGenerated by Electron Transfer Atom Transfer Radical Polymerization (ARGET-ATRP). The AMA allyl groups are not activated during copolymerization due to lower reactivity compared to the methacrylate groups, as demonstrated via ^{1}H-NMR spectroscopy (Fig. S1) and as seen in previous work. (Lounder and Asatekin, 2021) The allyl groups enabled cross-linking of the copolymer after membrane fabrication (Fig. 1; see Supporting Information for detailed experimental methods). AMA:SBMA monomer ratios were varied to synthesize one x-ZAC of intermediate ZI fraction (P-47) and two x-ZACs of high ZI fraction (P-72 and P-80), with the identifying number corresponding to the wt% ZI determined by ^{1}H-NMR (Fig. 1a, Fig. S1). P-72 and P-80 were expected to self-assemble form a network of ZI-rich nanodomains, similar to lower ZI content r-ZACs (Fig. 1b). (Bengani et al., 2015, Bengani-Lutz et al., 2017, Bengani-Lutz et al., 2017, Lounder and Asatekin, 2021, Bengani-Lutz et al., 2019, Lounder and Asatekin, 2021)

We characterized copolymer microphase separation using differential scanning calorimetry (DSC, Fig. 2). Microphase separated copolymers typically exhibit separate glass transition temperatures (T_gs) for each phase. (Mai and Eisenberg, 2012, Christie et al., 2018) However, due to the random copolymer architecture with short hydrophobic segments, the thermal relaxation of r-ZAC/x-ZAC hydrophobic domains can be suppressed until the zwitterionic groups are mobile. (Bengani-Lutz et al., 2017, Lounder and Asatekin, 2021, Ehrmann et al., 1992) Therefore, microphase separated r-ZACs possess T_gs significantly greater than the expected T_gs for homogeneously mixed copolymers, calculated

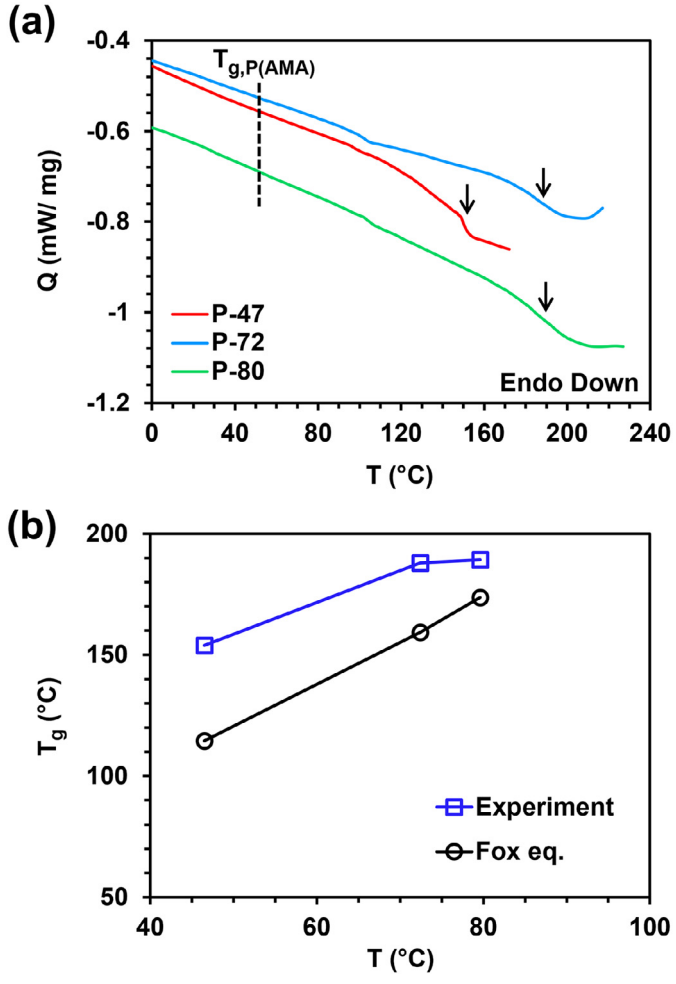

Fig. 2. (a) Differential scanning calorimetry (DSC) thermograms for P-47, P-72, and P-80. The glass transition temperatures (T_gs) are indicated with arrows. (b) Experimentally determined copolymer T_gs and Fox equation predictions vs. copolymer composition.

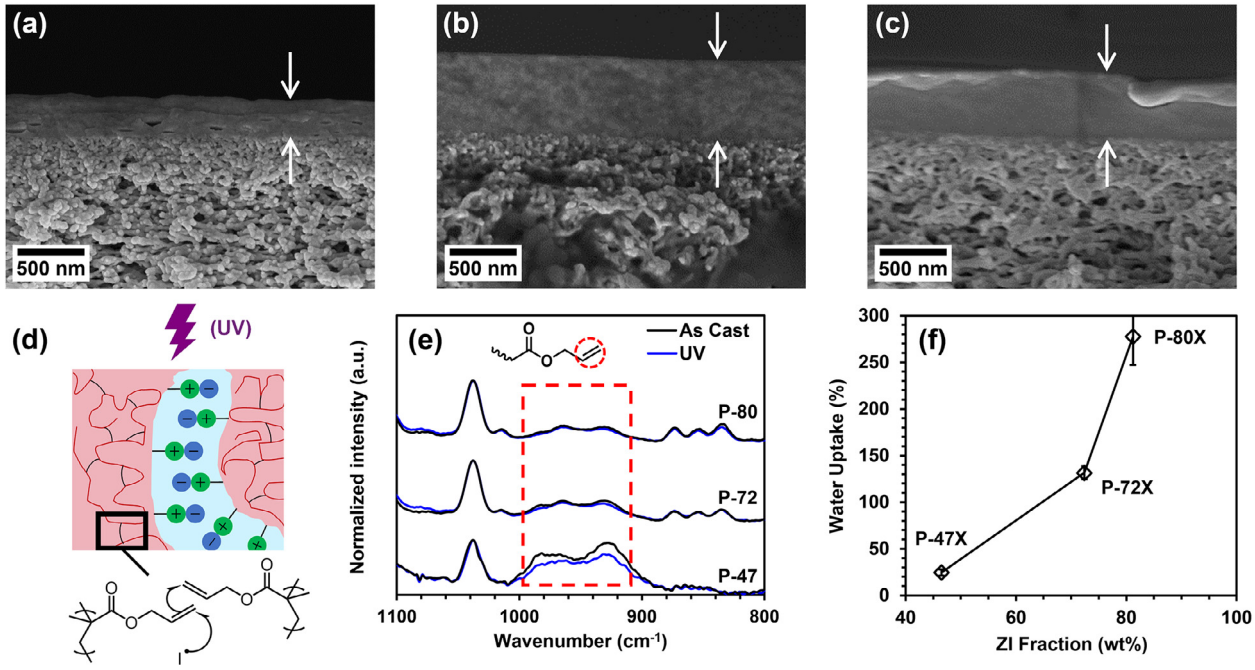

Fig. 3. (a-c) Cross-sectional FESEM images for (a) P-47, (b) P-72, and (c) P-80 TFC membranes. (d) Schematic illustration of copolymer cross-linking. UV light activates the radical initiator, which then cross-links the x-ZAC selective layer through radical polymerization of the AMA repeat units. (e) ATR-FTIR spectra for as-cast and UV-treated TFC membranes. The characteristic allyl peak (Vardareli̇ et al., 2008) is indicated by the dashed red box. (f) Water uptake vs. copolymer composition for cross-linked copolymer films.

by the Fox equation (Eq. S1). This was observed for P-47 and P-72, implying the formation of ZI-rich nanodomains. (Bengani-Lutz et al., 2017, Lounder and Asatekin, 2021, Ehrmann et al., 1992) The T_g of P-80 also exceeded the Fox equation prediction, although less than P-47 and P-72. While this possibly suggests less extensive phase separation, there is limited research involving r-ZACs of such high ZI fraction.

We prepared TFC membranes by rod-coating 3 wt/v% solutions of P(AMA-*r*-SBMA) in trifluoroethanol (TFE) onto a porous ultrafiltration membrane support (PS35, Solecta). TFE was selected because it is a good solvent for poly(zwitterions) and zwitterionic copolymers. (Laschewsky, 2014) We then used a heat gun to blow hot air across the membrane surface and rapidly evaporate the solvent. This method is simple and compatible with existing large-scale manufacturing technologies. (Lounder and Asatekin, 2021, Lounder and Asatekin, 2021) The resultant TFC membranes had thin (~300 – 600 nm) selective layers, as indicated by field emission scanning electron microscopy (FESEM) cross-sectional images (Fig. 3a-c). Previous P-47 membranes (Lounder and Asatekin, 2021, Lounder and Asatekin, 2021) had selective layer thicknesses of 440 ± 152 nm, suggesting that all three TFC membranes might have similar selective layer thicknesses due to the similar casting method.

To perform cross-linking, we equilibrated copolymer films or TFC membranes with a 3 w/v% solution of the photo-initiator (2-hydroxy-2-methylpropiophenone) in isopropanol and then shined UV light for 20 minutes (Fig. S2). (Lounder and Asatekin, 2021, Lounder and Asatekin, 2021) This initiated radical polymerization to cross-link the AMA units (Fig. 3d). Cross-linked P-47, P-72, and P-80 are identified as P-47X, P-72X, and P-80X, respectively. The covalent cross-links limited aqueous swelling of the copolymers in water. (Lounder and Asatekin, 2021) Cross-linking was essential to prevent instability through solvation or excessive swelling of the extremely hydrophilic P-72 and P-80 membranes (Fig. S3-S5).

We characterized the cross-linking chemistry using attenuated total reflectance Fourier transform infrared spectroscopy (ATR-FTIR). The intensity of the allyl peak region (980-930 cm^{-1}) decreased upon cross-linking (Fig. 3e), corresponding to conversion of the allyl groups. (Vardareli̇ et al., 2008) We performed peak integration with consistently selected baselines to roughly calculate the fraction of cross-linked allyl groups, estimating 25%, 18%, and 15% for P-47X, P-72X, and P-80X, respectively (Fig. S6). Since a higher fraction of cross-linked AMA groups corresponded to copolymers of higher AMA content, the total mole fraction of cross-linked monomers decreased significantly with increasing ZI content.

We next measured the water uptake of P-47X P-72X, and P-80X cross-linked films (Fig. 3f). Water uptake increased drastically with ZI fraction, likely due to greater hydrophilicity and lower degree of cross-linking. P-72X and P-80X demonstrated water uptakes of 129% and 288%, respectively, ~3–7 times greater than that of previous un-cross-linked r-ZACs. (Bengani et al., 2015) The high ZI content x-ZAC selective layers were likely soft compared to previous r-ZACs due to high water uptake. Nonetheless, ZI nanochannel compaction is not anticipated since nanochannels are not formed by empty, collapsible pores, but hydrated zwitterions. These sorption characteristics likely extend to other hydrophilic species (*e.g.* ionic liquids). This suggests that high ZI content x-ZACs could be used for applications beyond membrane filtration such as designing solid-state devices for electrical energy storage. (Taylor et al., 2020, Clark et al., 2020, Lind et al., 2016, Brown et al., 2010)

We investigated the effect of ZI fraction on membrane performance using dead-end filtration experiments. Effective membrane pore size was determined by filtering a series of neutral solutes at 7 L m^{-2} hr^{-1} operating flux and fitting rejection data to the Donnan Steric Pore Model (Lounder and Asatekin, 2021, Bowen and Mohammad, 1998, Hatakeyama et al., 2011) (Fig. 4a, Table S3). Cross-linked P-47X and un-cross-linked P-47 demonstrated pore sizes of 0.9 nm and 1.4 nm, respectively, representing the previously accessible selectivity range for P(AMA-*r*-SBMA) membranes cross-linked to varying degrees. (Lounder and Asatekin, 2021) The P-72X and P-80X membranes had effective pore sizes of 1.5 and 1.8 nm, respectively, well outside this previous range. These pore sizes are smaller than those of typical cross-

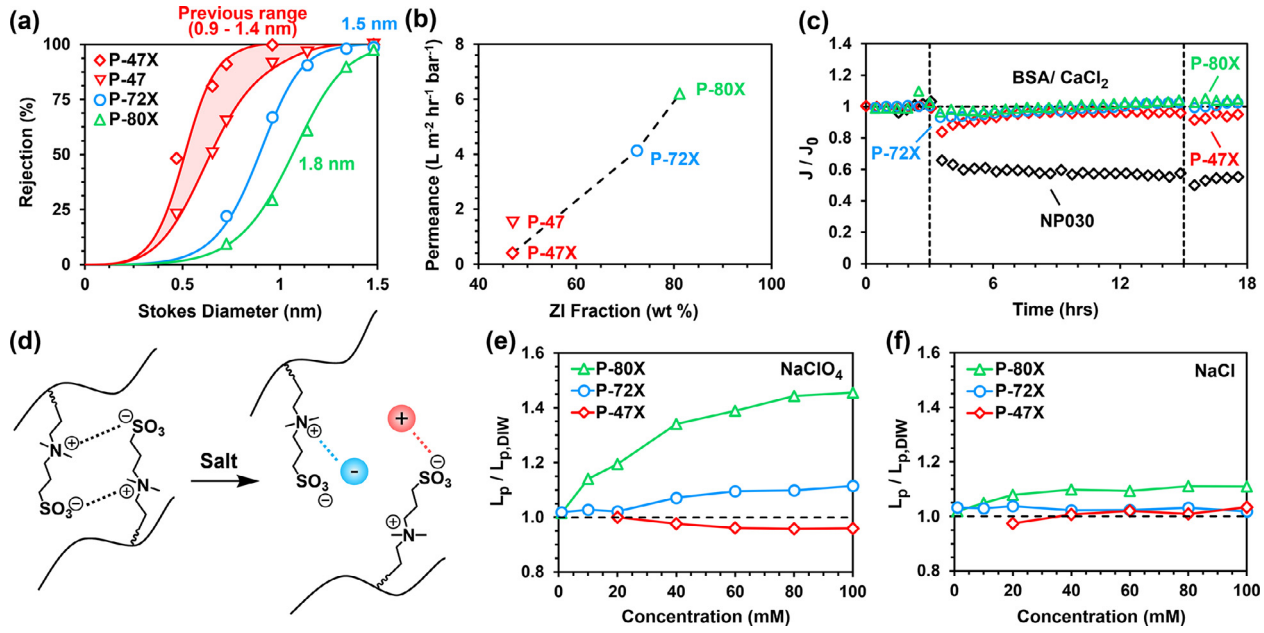

Fig. 4. (a) Rejection of neutral solutes vs. Stokes diameter, and best fit to the Donnan Steric Pore Model (solid lines). In order of decreasing size, the solutes were vitamin B12, α-cyclodextrin, raffinose, sucrose, glucose, xylose, and glycerol. The previous pore size range accessible with P(AMA-*r*-SBMA) membranes (Lounder and Asatekin, 2021) is highlighted in pink. (b) Membrane pure water permeance vs. copolymer composition. (c) Fouling of three x-ZAC membranes and a commercial nanofiltration membrane (NP030) with a protein solution (1000 ppm BSA/ 10 mM $CaCl_2$, pH 6.3). Flux (J) normalized by initial flux while filtering the background electrolyte solution (J_0=10 $Lm^{-2}hr^{-1}$) is shown over time while filtering the foulant solution and then after a gentle rinse. (d) Schematic illustration of the anti-polyelectrolyte effect. ZI-ZI complexes are broken by competing ZI-ion complexes, leading to increased zwitterionic domain swelling. (e-f) Membrane permeance in the presence of salt solutions (L_p) normalized by the pure water permeance ($L_{p,DIW}$) for (e) $NaClO_4$ and (f) NaCl at varying concentrations.

linked hydrogels, (Axpe et al., 2019, Le et al., 2017, Xiao et al., 2021, Quilitzsch et al., 2016, Sadeghi et al., 2018) accessed here through the high ZI content copolymer chemistry. In previous r-ZAC membranes containing 30-50 wt% ZI, pore size was independent of ZI content, likely due to the percolated, rigid and bicontinuous hydrophobic domain that constrains swelling. (Bengani et al., 2015) Somewhere between 50-72 wt% ZI, the hydrophobic domains likely lose this percolation, allowing greater expansion of the ZI domains in water, consistent with the extensive water uptake (Fig. 3f). As a result, high ZI content x-ZACs can be used to access new separations. For example, the low glucose and sucrose retention by the P-80X membranes suggest they could be used for ultrafiltration applications such as the separation of proteins from mono-/ disaccharides, (Galanakis et al., 2014) not possible with the P-47 and P-47X membranes. High ZI x-ZACs with shorter cross-linking times can potentially access even larger effective pore sizes.

For r-ZAC membranes with 30-50 wt% ZI units, permeance increases in direct proportion with ZI weight fraction as higher ZI content increases the number of equally sized nanochannels. (Bengani et al., 2015) Permeance increased much more dramatically with ZI fraction for the high ZI content x-ZAC membranes, however, likely due to the simultaneous increase in both the size and the interconnectivity of the ZI domains (Fig. 4b). Hydraulic water permeability, a thickness-normalized metric, increased even more dramatically with ZI content (Fig. S7, Table S4). This was because hydrated selective layer thickness also increased with ZI content due to greater water uptake (Fig. 3f).

To quantify the resistance of these highly hydrophilic x-ZAC membranes to fouling, we challenged the P-47X, P-72X, and P-80X membranes with a model foulant solution comprising 1000 ppm bovine serum albumin (BSA) in 10 mM $CaCl_2$ at pH 6.3 (Fig. 4c). P-47X membranes demonstrated excellent fouling resistance, particularly compared with the commercial nanofiltration membrane NP030, retaining ~95% of its flux during foulant filtration. This ~5% loss in permeance was not recovered after a gentle rinse. The P-72X and P-80X membranes, in contrast, demonstrated no loss in flux at any point during the fouling experiment. This is likely due to greater concentration of ZI groups on the selective layer surface, leading to increased hydrophilicity. We also examined membrane stability after 24 hours of exposure to buffers ranging pH 3-11 (Fig. S8). ATR-FTIR spectra indicated no change to the carbonyl bond chemistry, confirming that ester hydrolysis (Schonemann et al., 2018) did not occur.

In deionized water, ZI polymers form ZI-ZI complexes. These are broken in the presence of salt ions that shield their interactions. This phenomenon, termed the anti-polyelectrolyte effect, results in increased swelling and solubility of ZI polymers or domains at higher ionic strength (Fig. 4d). (Schlenoff, 2014, Wang et al., 2013) This ionic strength response has been observed in some membranes that feature zwitterionic polymer brushes. (Kaner et al., 2019, Birkner and Ulbricht, 2015, Zhao et al., 2016, Zhai et al., 2003) We have not observed salt responsive behavior for ZAC-based membranes with <50 wt% ZI groups in a preliminary study, (Kou, 2016) however, likely because the fully percolated hydrophobic domain serves as a rigid framework that prevents the ZI domain from swelling. To determine if the cross-linked x-ZAC membranes exhibit salt-responsiveness through the anti-polyelectrolyte effect, we measured membrane permeance while filtering aqueous solutions of $NaClO_4$ (Fig. 4e) and NaCl (Fig. 4f) at varying concentrations. $NaClO_4$ increases swelling of grafted P(SBMA) chains to a greater extent than NaCl, (Lounder and Asatekin, 2021, Wang et al., 2013) and is thus expected to cause a stronger response.

Neither salt led to increased permeance for the P-47X membranes, likely because the ZI domains were arrested by the fully percolated/ cross-linked hydrophobic domain. (Lounder and Asatekin, 2021) Interestingly, we observed a slight (~4%) permeance decrease in the presence of $NaClO_4$. P-47X absorbs $NaClO_4$ extensively, (Lounder and Asatekin, 2021) so it is possible that the salt ions occupied space in the zwitterionic nanochannels and reduced their effective size and permeability. (Dischinger et al., 2017)

In contrast, the permeances of the high ZI content P-72X and P-80X membranes increased with increasing $NaClO_4$ concentration (Fig. 4e),

as vitamin B12 rejection also decreased (Fig. S9). These changes were fully reversible, with the membranes recovering initial permeance (Fig. S4) and selectivity (Fig. S5) after returning to DIW. This suggests that $NaClO_4$ solutions further swell the ZI channels, leading to increased permeance and pore size. This reflects greater mobility of the ZI domains compared to previous ZAC-based membranes with <50 wt% ZI. (Bengani et al., 2015, Bengani-Lutz et al., 2017, Bengani-Lutz et al., 2017, Lounder and Asatekin, 2021, Lounder and Asatekin, 2021) The P-80X membranes showed a greater permeance increase than the P-72X membranes due to their greater ZI fraction and lower confinement by AMA domains. Similar permeance trends were observed for P-72X and P-80X membranes in the presence of NaCl (Fig. 4f), although permeance increased less significantly with NaCl than $NaClO_4$, consistent with relative interaction strengths of SBMA with each ion. (Lounder and Asatekin, 2021, Wang et al., 2013) Permeance also increased slightly while filtering the background electrolyte solution ($CaCl_{2(aq)}$) during the fouling experiment (Table S5). This was likely accompanied by a very slight increase in effective pore size, although BSA rejection is still expected to be ~100% due to its large size. (Axelsson, 1978)

This study demonstrates a new approach for synthesizing extremely fouling-resistant, zwitterionic membranes with controlled, tunable pore sizes that extend from ion separations (<1 nm) to the ultrafiltration range (~2 nm). This is achieved by the cross-linking of specially designed x-ZACs that contain a high fraction of ZI monomers, otherwise unusable in membrane manufacture due to their solubility in water. We found that membrane pore size and permeance increased with ZI fraction, and that the high ZI content membranes demonstrated exceptional resistance to protein fouling. Interestingly, the high ZI content membranes also demonstrated a salt-responsive behavior driven by the anti-polyelectrolyte effect. These new findings can be further extended to even higher effective pore sizes by changing cross-linking times or by utilizing alternative cross-linking schemes. Coupled with ionic strength responsive behavior, the effective pore size can be tuned over a broad range, accessing separations in the ultrafiltration range, including challenging protein separations.

Acknowledgements

We gratefully acknowledge financial support from the National Science Foundation grant number CBET-1553661, the Department of Energy grant number DE-DEFE003185 (led by ZwitterCo, Inc.), and the 2020-2021 Environmental Research Fellowship offered by Tufts University's Institute of the Environment. FESEM images were collected at the Harvard Center for Nanoscale Systems (Harvard CNS). We thank Solecta for donating support membranes. A.A. thanks Chris Drover for helpful conversations.

Declaration of Competing Interest

Ayse Asatekin owns a minor equity in and serves as the Senior Scientific Advisor of ZwitterCo. Inc., which was the lead institution in the NSF grant IIP-1843847 that partially funded this work. ZwitterCo also holds a license from Tufts University to commercialize the technology described in this manuscript. Other authors declare no conflict of interest.

The authors declare the following financial interests/personal relationships which may be considered as potential competing interests:

Ayse Asatekin reports financial support was provided by ZwitterCo, Inc. Ayse Asatekin reports financial support was provided by National Science Foundation. Ayse Asatekin reports financial support was provided by US Department of Energy. Ayse Asatekin reports a relationship with ZwitterCo, Inc. that includes: board membership, equity or stocks, and funding grants. Ayse Asatekin has patent Cross-linkable Zwitterionic Polymers and Their Use in Membrane Filters pending to ZwitterCo, Inc. Ayse Asatekin owns a small equity in and serves as the Senior Scientific Advisor to ZwitterCo, Inc., which was the lead institution in the Department of Energy grant DE-DEFE003185, which partially funded this work. A patent application derived from this work, as well as other potentially relevant patents, are optioned or licenced by ZwitterCo, Inc.

Supplementary materials

Supplementary data associated with this article can be found, in the online version, at doi:10.1016/j.memlet.2022.100019.

References

Bruggen, B.V.d., Vandecasteele, C., 2003. Removal of pollutants from surface water and groundwater by nanofiltration: overview of possible applications in the drinking water industry. Environmental Pollution 122 (3), 435–445.
Epsztein, R., DuChanois, R.M., Ritt, C.L., Noy, A., Elimelech, M., 2020. Towards single-species selectivity of membranes with subnanometre pores. Nature Nanotechnology 15 (6), 426–436.
Greenlee, L.F., Lawler, D.F., Freeman, B.D., Marrot, B., Moulin, P., 2009. Reverse osmosis desalination: water sources, technology, and today's challenges. Water Res 43 (9), 2317–2348.
Mauter, M.S., Zucker, I., Perreault, F.o., Werber, J.R., Kim, J.-H., Elimelech, M., 2018. The role of nanotechnology in tackling global water challenges. Nature Sustainability 1 (4), 166–175.
Shannon, M.A., Bohn, P.W., Elimelech, M., Georgiadis, J.G., Marinas, B.J., Mayes, A.M., 2008. Science and technology for water purification in the coming decades. Nature 452 (7185), 301–310.
Sholl, D.S., Lively, R.P., 2016. Seven chemical separations to change the world. Nature 532, 435–437.
Zhang, R., Liu, Y., He, M., Su, Y., Zhao, X., Elimelech, M., Jiang, Z., 2016. Antifouling membranes for sustainable water purification: strategies and mechanisms. Chemical Society Reviews 45 (21), 5888–5924.
Hurwitz, G., Bhattacharjee, S., Seo, E., Wang, J., Severt, A., Temple, J., Nguyen, J., Koehler, J., Hoek, E.M.V., 2018. Field testing of PolyCera®, PES, and PVDF ultrafiltration membranes in municipal tertiary filtration: impacts of membrane polymer chemistry on fouling, cleaning, energy, and cost. Desalination and Water Treatment 111, 39–47.
Esfahani, M.R., Aktij, S.A., Dabaghian, Z., Firouzjaei, M.D., Rahimpour, A., Eke, J., Escobar, I.C., Abolhassani, M., Greenlee, L.F., Esfahani, A.R., Sadmani, A., Koutahzadeh, N., 2019. Nanocomposite membranes for water separation and purification: Fabrication, modification, and applications. Separation and Purification Technology 213, 465–499.
Ward, L.M., Fickling, B.G., Weinman, S.T., 2021. Effect of Nanopatterning on Concentration Polarization during Nanofiltration. Membranes (12) 11.
Maan, A.M.C., Hofman, A.H., Vos, W.M., Kamperman, M., 2020. Recent Developments and Practical Feasibility of Polymer-Based Antifouling Coatings. Advanced Functional Materials 30 (32).
Laschewsky, A., 2014. Structures and Synthesis of Zwitterionic Polymers. Polymers 6 (5), 1544–1601.
Bhattacharya, A., Misra, B.N., 2004. Grafting: a versatile means to modify polymersTechniques, factors and applications. Progress in Polymer Science 29 (8), 767–814.
Susanto, H., Ulbricht, M., 2007. Photografted Thin Polymer Hydrogel Layers on PES Ultrafiltration Membranes: Characterization, Stability, and Influence on Separation Performance. Langmuir 23 (14), 7818–7830.
Shahkaramipour, N., Ramanan, S.N., Fister, D., Park, E., Venna, S.R., Sun, H., Cheng, C., Lin, H., 2017. Facile Grafting of Zwitterions onto the Membrane Surface To Enhance Antifouling Properties for Wastewater Reuse. Industrial & Engineering Chemistry Research 56 (32), 9202–9212.
Yang, R., Xu, J., Ozaydin-Ince, G., Wong, S.Y., Gleason, K.K., 2011. Surface-Tethered Zwitterionic Ultrathin Antifouling Coatings on Reverse Osmosis Membranes by Initiated Chemical Vapor Deposition. Chemistry of Materials 23 (5), 1263–1272.
Weinman, S.T., Bass, M., Pandit, S., Herzberg, M., Freger, V., Husson, S.M., 2018. A switchable zwitterionic membrane surface chemistry for biofouling control. Journal of Membrane Science 548, 490–501.
Kaner, P., Dudchenko, A.V., Mauter, M.S., Asatekin, A., 2019. Zwitterionic copolymer additive architecture affects membrane performance: fouling resistance and surface rearrangement in saline solutions. Journal of Materials Chemistry A 7 (9), 4829–4846.
Kaner, P., Hu, X., Thomas, S.W., Asatekin, A., 2017. Self-Cleaning Membranes from Comb-Shaped Copolymers with Photoresponsive Side Groups. ACS Applied Materials and Interfaces 9 (15), 13619–13631.
Sun, Q., Su, Y., Ma, X., Wang, Y., Jiang, Z., 2006. Improved antifouling property of zwitterionic ultrafiltration membrane composed of acrylonitrile and sulfobetaine copolymer. Journal of Membrane Science 285 (1-2), 299–305.
Zhao, X., Chen, W., Su, Y., Zhu, W., Peng, J., Jiang, Z., Kong, L., Li, Y., Liu, J., 2013. Hierarchically engineered membrane surfaces with superior antifouling and self-cleaning properties. Journal of Membrane Science 441, 93–101.
Sadeghi, I., Kaner, P., Asatekin, A., 2018. Controlling and Expanding the Selectivity of Filtration Membranes. Chemistry of Materials 30 (21), 7328–7354.
Zhang, Y., Almodovar-Arbelo, N.E., Weidman, J.L., Corti, D.S., Boudouris, B.W., Phillip, W.A., 2018. Fit-for-purpose block polymer membranes molecularly engineered for water treatment. npj Clean Water 1 (2), 1–14.
Sujanani, R., Landsman, M.R., Jiao, S., Moon, J.D., Shell, M.S., Lawler, D.F., Katz, L.E., Freeman, B.D., 2020. Designing Solute-Tailored Selectivity in Membranes: Perspectives for Water Reuse and Resource Recovery. ACS Macro Letters 9 (11), 1709–1717.

Guillen, G.R., Pan, Y., Li, M., Hoek, E.M.V., 2011. Preparation and Characterization of Membranes Formed by Nonsolvent Induced Phase Separation: A Review. Industrial & Engineering Chemistry Research 50 (7), 3798–3817.
Dong, X., Jeong, T.J., Kline, E., Banks, L., Grulke, E., Harris, T., Escobar, I.C., 2020. Eco-friendly solvents and their mixture for the fabrication of polysulfone ultrafiltration membranes: An investigation of doctor blade and slot die casting methods. Journal of Membrane Science 614.
Lang, C., Kumar, M., Hickey, R.J., 2021. Current status and future directions of self--assembled block copolymer membranes for molecular separations. Soft Matter 17 (46), 10405–10415.
Moon, J.D., Freeman, B.D., Hawker, C.J., Segalman, R.A., 2020. Can Self-Assembly Address the Permeability/Selectivity Trade-Offs in Polymer Membranes? Macromolecules 53 (14), 5649–5654.
Hoffman, J.R., Phillip, W.A., 2020. Dual-Functional Nanofiltration Membranes Exhibit Multifaceted Ion Rejection and Antifouling Performance. ACS Applied Materials and Interfaces 12 (17), 19944–19954.
Zhang, Y., Mulvenna, R.A., Qu, S., Boudouris, B.W., Phillip, W., 2017. Block Polymer Membranes Functionalized with Nanoconfined Polyelectrolyte Brushes Achieve Sub–Nanometer Selectivity. ACS Macro Letters 6 (7), 726–732.
Sadeghi, I., Kronenberg, J., Asatekin, A., 2018. Selective Transport through Membranes with Charged Nanochannels Formed by Scalable Self-Assembly of Random Copolymer Micelles. ACS Nano 12, 95–108.
Sadeghi, I., Asatekin, A., 2019. Membranes with Functionalized Nanopores for Aromaticity-Based Separation of Small Molecules. ACS Applied Materials & Interfaces 11 (13), 12854–12862.
Qu, S., Dilenschneider, T., Phillip, W.A., 2015. Preparation of Chemically-Tailored Copolymer Membranes with Tunable Ion Transport Properties. ACS Applied Materials and Interfaces 7 (35), 19746–19754.
Zhang, Z., Simon, A., Abetz, C., Held, M., Hohme, A.L., Schneider, E.S., Segal-Peretz, T., Abetz, V., 2021. Hybrid Organic-Inorganic-Organic Isoporous Membranes with Tunable Pore Sizes and Functionalities for Molecular Separation. Advanced Materials 33 (48), e2105251.
Zhang, Z., Rahman, M.M., Abetz, C., Hohme, A.L., Sperling, E., Abetz, V., 2020. Chemically Tailored Multifunctional Asymmetric Isoporous Triblock Terpolymer Membranes for Selective Transport. Advanced Materials 32 (8), e1907014.
Dugas, M.P., Van Every, G., Park, B., Hoffman, J.R., LaRue, R.J., Bush, A.M., Zhang, Y., Schaefer, J.L., Latulippe, D.R., Phillip, W.A., 2020. Resilient hollow fiber nanofiltration membranes fabricated from crosslinkable phase-separated copolymers. Molecular Systems Design & Engineering 5 (5), 943–953.
Bengani, P., Kou, Y., Asatekin, A., 2015. Zwitterionic copolymer self-assembly for fouling resistant, high flux membranes with size-based small molecule selectivity. Journal of Membrane Science 493, 755–765.
Bengani-Lutz, P., Converse, E., Cebe, P., Asatekin, A., 2017. Self-Assembling Zwitterionic Copolymers as Membrane Selective Layers with Excellent Fouling Resistance: Effect of Zwitterion Chemistry. ACS Applied Materials and Interfaces 9 (24), 20859–20872.
Bengani-Lutz, P., Zaf, R.D., Culfaz-Emecen, P.Z., Asatekin, A., 2017. Extremely fouling resistant zwitterionic copolymer membranes with ~ 1 nm pore size for treating municipal, oily and textile wastewater streams. Journal of Membrane Science 543, 184–194.
Lounder, S.J., Asatekin, A., 2021. Zwitterionic Ion-Selective Membranes with Tunable Subnanometer Pores and Excellent Fouling Resistance. Chemistry of Materials 33 (12), 4408–4416.
Bengani-Lutz, P., Sadeghi, I., Lounder, S.J., Panzer, M.J., Asatekin, A., 2019. High Flux Membranes with Ultrathin Zwitterionic Copolymer Selective Layers with ~1 nm Pores Using an Ionic Liquid Cosolvent. ACS Applied Polymer Materials 1 (8), 1954–1959.
Lounder, S.J., Asatekin, A., 2021. Interaction-based ion selectivity exhibited by self-assembled, cross-linked zwitterionic copolymer membranes. In: Proceedings of the National Academy of Sciences of the United States of America, 118.
Mai, Y., Eisenberg, A., 2012. Self-assembly of block copolymers. Chem Soc Rev 41 (18), 5969–5985.
Christie, D., Register, R.A., Priestley, R.D., 2018. Direct Measurement of the Local Glass Transition in Self-Assembled Copolymers with Nanometer Resolution. ACS Central Science 4 (4), 504–511.
Ehrmann, M., Mathis, A., Meurer, B., Scheer, M., Galin, J.C., 1992. Statistical n-Butyl Acrylate-(Sulfopropyl) ammonium Betaine Copolymers. 2. Structural Studies. Macromolecules 25 (8), 2253–2261.
Vardareli̇, T.K., Keski̇n, S., Usanmaz, A., 2008. Synthesis and Characterization of Poly(allyl methacrylate) Obtained by Free Radical Initiator. Journal of Macromolecular Science, Part A 45 (4), 302–311.
Taylor, M.E., Lounder, S.J., Asatekin, A., Panzer, M.J., 2020. Synthesis and Self-Assembly of Fully Zwitterionic Triblock Copolymers. ACS Materials Letters 2 (3), 261–265.
Clark, A., Taylor, M.E., Panzer, M.J., Cebe, P., 2020. Interactions between ionic liquid and fully zwitterionic copolymers probed using thermal analysis. Thermochimica Acta 691.
Lind, F., Rebollar, L., Bengani-Lutz, P., Asatekin, A., Panzer, M.J., 2016. Zwitterion-Containing Ionogel Electrolytes. Chemistry of Materials 28 (23), 8480–8483.
Brown, R.H., Duncan, A.J., Choi, J.H., Park, J.K., Wu, T., Leo, D.J., Winey, K.I., Moore, R.B., Long, T.E., 2010. Effect of ionic liquid on mechanical properties and morphology of zwitterionic copolymer membranes. Macromolecules 43 (2), 790–796.
Bowen, W.R., Mohammad, A.W., 1998. Diafiltration by nanofiltration: Prediction and optimization. AIChE Journal 44 (8), 1799–1812.
Hatakeyama, E.S., Gabriel, C.J., Wiesenauer, B.R., Lohr, J.L., Zhou, M., Noble, R.D., Gin, D.L., 2011. Water filtration performance of a lyotropic liquid crystal polymer membrane with uniform, sub-1-nm pores. Journal of Membrane Science 366 (1-2), 62–72.
Axpe, E., Chan, D., Offeddu, G.S., Chang, Y., Merida, D., Hernandez, H.L., Appel, E.A., 2019. A Multiscale Model for Solute Diffusion in Hydrogels. Macromolecules 52 (18), 6889–6897.
Le, N.L., Ulbricht, M., Nunes, S.P., 2017. How Do Polyethylene Glycol and Poly(sulfobetaine) Hydrogel Layers on Ultrafiltration Membranes Minimize Fouling and Stay Stable in Cleaning Chemicals? Industrial & Engineering Chemistry Research 56 (23), 6785–6795.
Xiao, Z., Zheng, X., An, Y., Wang, K., Zhang, J., He, H., Wu, J., 2021. Zwitterionic hydrogel for sustained release of growth factors to enhance wound healing. Biomaterials Science 9 (3), 882–891.
Quilitzsch, M., Osmond, R., Krug, M., Heijnen, M., Ulbricht, M., 2016. Macro-initiator mediated surface selective functionalization of ultrafiltration membranes with anti-fouling hydrogel layers applicable to ready-to-use capillary membrane modules. Journal of Membrane Science 518, 328–337.
Sadeghi, I., Yi, H., Asatekin, A., 2018. A Method for Manufacturing Membranes with Ultrathin Hydrogel Selective Layers for Protein Purification: Interfacially Initiated Free Radical Polymerization (IIFRP). Chemistry of Materials 30 (4), 1265–1276.
Galanakis, C.M., Chasiotis, S., Botsaris, G., Gekas, V., 2014. Separation and recovery of proteins and sugars from Halloumi cheese whey. Food Research International 65, 477–483.
Schonemann, E., Laschewsky, A., Rosenhahn, A., 2018. Exploring the Long-Term Hydrolytic Behavior of Zwitterionic Polymethacrylates and Polymethacrylamides. Polymers (Basel) 10 (6), 639.
Schlenoff, J.B., 2014. Zwitteration: Coating Surfaces with Zwitterionic Functionality to Reduce Nonspecific Adsorption. Langmuir 30 (32), 9625–9636.
Wang, T., Wang, X., Long, Y., Liu, G., Zhang, G., 2013. Ion-Specific Conformational Behavior of Polyzwitterionic Brushes: Exploiting It for Protein Adsorption/Desorption Control. Langmuir 29 (22), 6588–6596.
Birkner, M., Ulbricht, M., 2015. Ultrafiltration membranes with markedly different pH- and ion-responsivity by photografted zwitterionic polysulfobetain or polycarbobetain. Journal of Membrane Science 494, 57–67.
Zhao, Y.-F., Zhang, P.-B., Sun, J., Liu, C.-J., Zhu, L.-P., Xu, Y.-Y., 2016. Electrolyte-responsive polyethersulfone membranes with zwitterionic polyethersulfone-based copolymers as additive. Journal of Membrane Science 510, 306–313.
Zhai, G., Toh, S.C., Tan, W.L., Kang, E.T., Neoh, K.G., Huang, C.C., Liaw, D.J., 2003. Poly(vinylidene fluoride) with Grafted Zwitterionic Polymer Side Chains for Electrolyte-Responsive Microfiltration Membranes. Langmuir 19 (17), 7030–7037.
Kou, Y., 2016. Ionic Strength of Zwitterionic Polymer Membranes. Tufts University. Digital Collections and Archives..
Dischinger, S.M., McGrath, M.J., Bourland, K.R., Noble, R.D., Gin, D.L., 2017. Effect of post-polymerization anion-exchange on the rejection of uncharged aqueous solutes in nanoporous, ionic, lyotropic liquid crystal polymer membranes. Journal of Membrane Science 529 (December 2016), 72–79.
Axelsson, I., 1978. Characterization of Proteins and Other Macromolecules by Agarose Gel Chromatography. Journal of Chromatography 152, 21–32.